MULTIBODY DYNAMICS 2011, ECCOMAS Thematic Conference
J.C. Samin, P. Fisette (eds.)
Brussels, Belgium, 4-7 July 2011

MULTIBODY SIMULATION OF TIRES OPERATING ON AN UNEVEN ROAD

Louis Gagnon[⋆], Marc J. Richard[⋆], Pierangelo Masarati[†], Marco Morandini[†], and Guy Doré[∗]

[⋆]Département de Génie Mécanique
Université Laval, 1065, de la Médecine, Québec (QC) G1V 0A6 Canada
e-mails: Louis.Gagnon.10@ulaval.ca, Marc.Richard@gmc.ulaval.ca

[†]Dipartimento di Ingegneria Aerospaziale
Politecnico di Milano, Via La Masa 34, 20156 Milano, Italia
e-mails: Pierangelo.Masarati@polimi.it, Marco.Morandini@polimi.it

[∗]Département de Génie Civil
Université Laval, 1065, de la Médecine, Québec (QC) G1V 0A6 Canada
e-mail: Guy.Dore@gci.ulaval.ca

Keywords: Truck-road interaction, Rigid ring tire model, Open-source multibody software, Magic formula, Implicit integration, Road unevenness.

Abstract. *In this paper a tire model is developed within an open-source multibody software for the purpose of accurately evaluating the energy demand of a truck traveling on a real road profile while also giving the proper dynamic properties of the tire responses. This model will be used in a multibody tractor-trailer simulation to properly evaluate the fuel consumption and wear of the vehicle and the safety, comfort, and health of the driver. The model consists of an implementation of a rigid ring tire model tailored to applications at low camber angles, limited steering and velocity changes, and continuous contact with the road. A broad range of road wavelengths and frequencies are to be studied. A qualitative validation of the model is done using a wheel attached to a fixed axle to reproduce experimental settings. This validation shows that the model behaves as is expected from a typical rigid ring model while driving on uneven road surfaces. Another validation procedure is done with both simple and complex tractor models and shows that the steer inputs to the model respond as a rigid ring model is expected to and that the magic formulae properties are reproduced adequately for disturbances of low frequencies, as expected.*

ISBN 978-2-8052-0116-5

1 INTRODUCTION

A Multibody dynamic model is developed to simulate the behavior of an eighteen wheel semi-trailer truck driving on an uneven road. The objective is to gather information that will assess the influence of the road profile on the fuel consumption; the safety; the wear of the truck; and the health of the driver. The model is built using exclusively free software.

Initially, two simulations were performed in order to assess the ability of the *MBDyn* multibody software to resolve the behavior of a car. These simulations are a *Reference Quarter Car Simulation* (RQCS) and a two wheel bicycle simulation with lateral and longitudinal tire forces. The latter model helps to evaluate the ability of *MBDyn* to handle the tire contact forces between the road and the vehicle.

The focus of the project is to implement and validate, in an open-source software, a rigid ring tire model largely inspired by the *Short Wavelength Intermediate Frequency Tire* (SWIFT) model, as discussed by Pacejka [7]. The model is also inspired by the descriptions of rigid ring models that are given by Schmeitz [9], by Maurice [6], and by Zegelaar [10]. The model is presented in this paper and two validation procedures are conducted and discussed.

2 FIRST ATTEMPTS

2.1 Energy Dissipated by the *Reference Quarter Car Model*

The RQCS is a simple quarter car model and is described by Sayers [8]. Its geometry is shown in Fig. (2). The response amplitude of the chassis to sinusoidal oscillations of the road at different frequencies is measured and compared with the results of Sayers [8]. The correlation is shown in Fig. (1). The energy input to the RQCS model is calculated because the energy consumption of the truck model will be assessed in a similar fashion. It is obtained from the dissipation of the viscous elements of the multibody model. A plot of the accumulated energy dissipation of the RQCS is shown in Fig. (3). One can notice the expected behavior that the total energy dissipated increases with time. The oscillations in the absorbed energy come from the fact that the spring element of the suspension absorbs and releases a constant amount of energy over each cycle. This test is done on a sinusoidal road profile with a frequency of one hertz and an amplitude of six centimeters. The large onset energy absorption is due to the suspended mass, m_s, being above the average equilibrium position at the initial time. The calculation is done according to the following formula, $\sum\{F_{sd} \cdot (\dot{y}_t - \dot{y}_s)\Delta t\}$, where Δt is the time step length, F_{sd} is the compression force of the spring and damper of the suspension, and $\dot{y}_t$ and $\dot{y}_s$ are the vertical velocities of the axle and suspended masses, respectively.

2.2 A Bicycle Model for Tire Forces

A two wheel model, constrained to movement in the yaw and planar degrees of freedom is developed using the currently available *MBDyn* elements. A lane change at fifty-nine kilometers per hour is simulated in order to validate the bicycle model and the results agree with the expected behavior. For example, at the onset of the lane change, the yaw angular acceleration of the body results from the forces applied at the wheels. The steer angle imposed on the front wheel is shown in Fig. (4). The yaw angle acceleration of the center of gravity of the vehicle body is plotted in Fig. (5). The y-components, in the global reference frame, of the lateral tire forces on the front and rear wheels, are plotted in Figs. (6) and (7), respectively.

ISBN 978-2-8052-0116-5

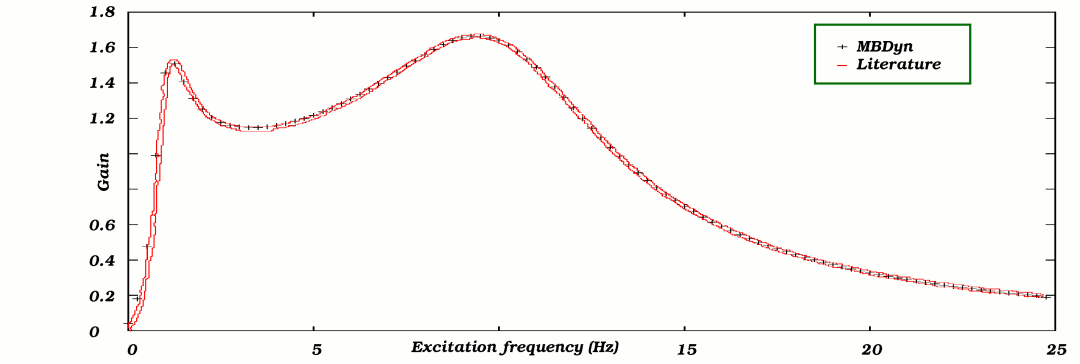

Figure 1: Frequency response of the RQCS.

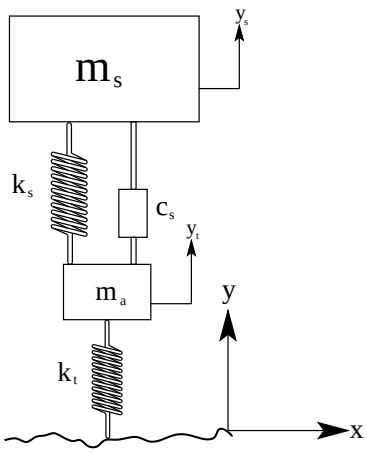

Figure 2: The RQCS.

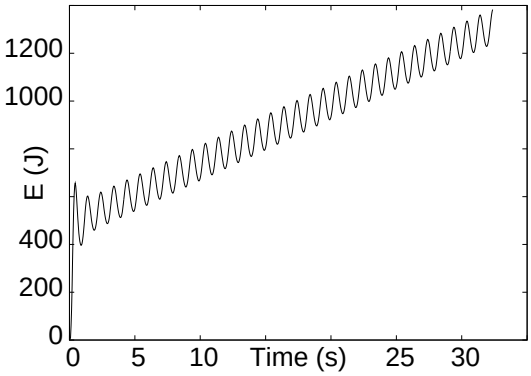

Figure 3: Energy dissipated by the RQCS.

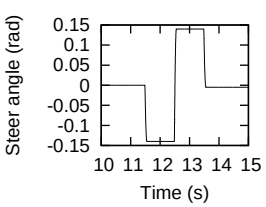

Figure 4: Steer angle.

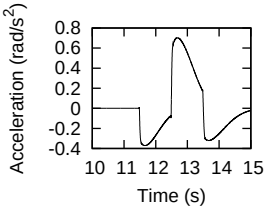

Figure 5: Body yaw.

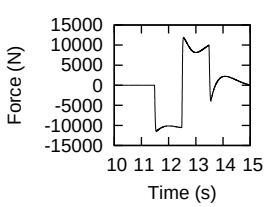

Figure 6: Front wheel.

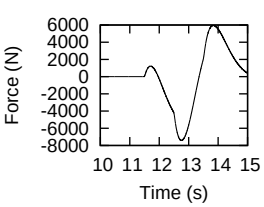

Figure 7: Rear wheel.

ISBN 978-2-8052-0116-5

3 RIGID RING TIRE MODEL

The choice of tire model was considered to be of uttermost importance in the development of the tractor-trailer model because the tires are expected to have an important effect on the dissipation of energy due to the small road profile irregularities. For that purpose a rigid ring model was deemed appropriate because of its proven capacity to model electronically controlled brake systems. This ability shows that the model has a good capacity to model the changes in energy of the vehicle traveling on an uneven road. A rigid ring type of model was also chosen due to its quick turnover time.

From the magic formula tire force model presented above, *MBDyn* is further enhanced in order to optimize the procedure and ease the implementation of a rigid ring tire model. A software module is developed to allow the introduction of eighteen wheels in a multibody analysis with almost as much ease as any other element. The truck model takes a left and a right surface profile, and a constant target velocity for input. The road profile inputs consist of both periodic and random longitudinal elevations of the left and right tracks of the road. The profiles have International Roughness Indices (IRI) ranging from one to five. Typical virtual profiles studied include rectangular and triangular bumps of different amplitudes and frequencies. Prior to feeding the profile to the model, it is filtered using a two point ellipsoid follower mechanism in order to smoothen road discontinuities, emulate the filtering action of the tire, and properly evaluate the slope of the profile. Both the height and the slope of the road are fed to the model after the filtering process. A physical representation of the model is shown in Fig. (8) where the wheel and contact patch lie inside the ring and below the ring, respectively. The positions of the elements are not relevant in that figure. The spring elements shown have both elastic and damping qualities and they are each unidirectional and independent of each other. In this situation the vehicle forces are transmitted from the truck to the wheel hub which transmits them to the ring which in turn transmits them to the contact patch. The contact patch is fixed to the ground at the height specified by the longitudinal road profile. This assumption excludes the possibility of properly modeling losses of contact between the road and the tire. Torsional viscoelastic elements are also present between the ring and the hub in each of the three coordinates and act independently of each other. The outer part of the rigid ring model, the wheel node, is connected to the vehicle by a revolute joint which means that it is only allowed to rotate along the lateral axis, and the steering axes for wheels that steer.

3.1 The Artificial Rotation

The contact patch node is given two degrees of freedom (DoF) in the model: one in the x-direction and one in the y-direction. Thus, the rotations in the x-y plane and in the road slope plane are taken into account by means of projections. The contact patch is assumed to always have the same orientation as the ring and this is as if it had a null moment of inertia. This method demands for a projection of the interaction force, between the ring and patch, and acting on the ring. This projection is governed by the normal direction to the ground, $\mathbf{n}$. In the artificial rotation method, the patch is never actually rotated and is also not subjected to gravity. Its mass is only used to model the delay in response of the tire that is present in a transient condition. Because the rotation is artificial, the patch has no moment of inertia and no angular springs are present between it and the ring. Thus, the aligning moment calculated from the magic formulae is applied directly on the ring but takes the lateral component of the interaction force between the ring and the patch as input in order to emulate the delay that would be given by an angular

ISBN 978-2-8052-0116-5

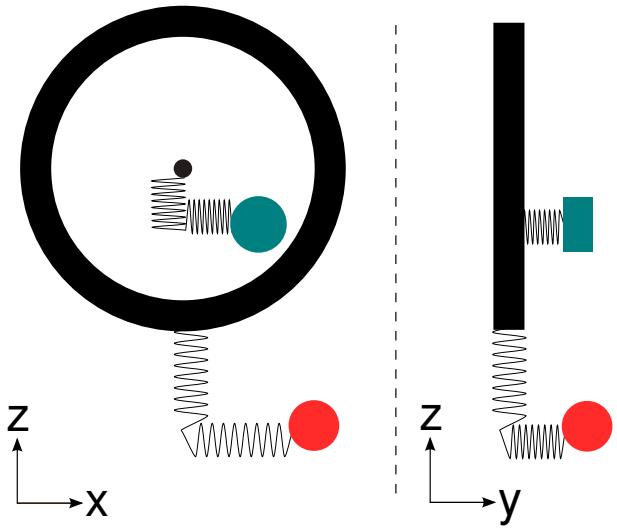

Figure 8: Representation of the elements of the tire model. Wheel hub is green, ring is black, and patch is red. Side view on the left and front view on the right.

spring used between patch and ring. Its formula is,

$$M_z = \mathbf{n}[-tr(\alpha)\mathbf{f}_{\mathbf{int,r}} \cdot \mathbf{j} + M_{zr}(\alpha)] \tag{1}$$

where M_z is the aligning moment applied to the ring, $tr(\alpha)$ is the pneumatic trail calculated from the magic formulae, $\mathbf{f}_{\mathbf{int,r}}$ is the force between the ring and the patch acting on the ring, thus projected according to the normal direction of the ground, $M_{zr}(\alpha)$ is the residual moment calculated from the magic formulae, and α is the lateral slip angle of the wheel.

The difference between the actual model, where both the contact patch and the ring share the same reference frame, and the physically obtained rotation of the contact patch by a projection of the interaction force between ring and patch along the normal and perpendicular directions is shown in Fig. (9).

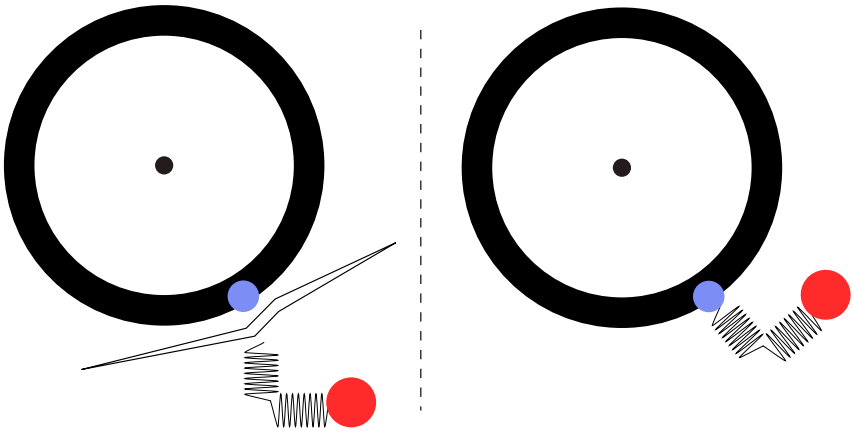

Figure 9: Representation of the artificial rotation used to properly direct the forces coming from the contact patch to the ring. Actual model on the left and model including the force projection on the right.

Other implications of the projection are the evaluation of the proper position on the longitudinal road profile, which is discussed in Sec. (3.5), and the evaluation of the physical distance

ISBN 978-2-8052-0116-5

between the ring center and the contact patch for the computation of the moment arm, which is discussed in Sec. (3.2).

Another thing to consider with the contact patch assumed to always follow the rotations of the ring is that the distances between ring and patch expressed in the absolute reference frame have x, y, and z that are actually expressed in the ring reference frame. Thus a projection is also done in order to keep the proper respective stiffness and damping coefficients of the patch in the two planar directions of the tire-ground contact. Without this precaution, the respective properties of the x- and y-directions of the tire would only be properly represented when the tire is moving straight ahead. For the same reason, a similar trick is used between the ring and the wheel nodes. The linear viscoelastic elements between those two nodes are defined between the ring and a non-rotating node attached to the wheel and sharing all of its other properties in order to have the x, y, and z coefficients follow the reference frame of the non-rotating node. It should be noted that this node can still rotate with steering and axle movements.

3.2 Moments

In this model, the forces are applied on the ring are considered to be acting at the position of the contact patch in an attempt to physically represent, using the contact patch relaxation viscoelastic elements, both the transient response delay to slip and slope variations and the position of the application of the forces on the ring. This is done in order to compute the aligning moment due to the lateral displacement of the contact patch and the application of the longitudinal force, the rolling resistance moment due to the longitudinal displacement of the contact patch and the vertical force, and the moment about the lateral axis due to the displacement of the contact patch in the vertical direction.

The rolling resistance moment due to the material properties of the tire, which is not taken into account by the damping present in the rigid ring model, is added to the ring as the product of a rolling resistance force and a distance equal to the distance between the center of the ring and the contact patch. This rolling resistance moment acts against the direction of rotation of the tire and is determined by the magic formulae. These formulae also serve to find the proper aligning torque moment due to the uneven pressure distribution along the longitudinal direction of the contact patch caused by the inherent properties of the tire, as can be interpreted from the brush model.

3.3 Effective Radius

The effective radius is here considered equal to the radius between the center of the wheel and the contact patch and is used for the calculation of the slip. The slip also takes into account the relative velocity between the wheel center and the contact patch, in the forward direction. Again, some projections have to be considered to properly evaluate this relative velocity. With this effective radius and relative velocity technique, it is expected that the physical slip ratio is accurately computed. The effect of velocity is not incorporated into the model because the tests are to be performed at constant velocity and the residual springs can be tuned accordingly. However, the idea of incorporating it in the future is considered since it might ease the correlation of results from simulations at various driving velocities.

3.4 Road Profile

Real road profiles are obtained from profilometer readings while virtual profiles are created numerically. Profiles are filtered before being fed to the rigid ring model. The filtering causes

ISBN 978-2-8052-0116-5

the response of the rigid ring model to road irregularities to be in line with the response of a real tire. The width of the contact patch is taken into account by a filtering done through the passage of a two-point follower on the already filtered profile. The two-point follower technique is performed on the profile already filtered by a rigid ellipsoid geometric function described in detail by Schmeitz [9]. The actual position on the longitudinal profile is obtained from,

$$x_g = \{\mathbf{p_c} - [(\mathbf{n} \times \mathbf{e}) \cdot \mathbf{i}]\mathbf{x_p}\} \cdot \mathbf{i} \tag{2}$$

and the two-point follower technique yields the following,

$$\mathbf{n} = \{[x_g + l_s, 0, R(x_g + l_s)] - [x_g - l_s, 0, R(x_g - l_s)]\} \times \mathbf{j}; \tag{3}$$

$$z_p = \frac{R(x_g + l_s) + R(x_g - l_s)}{2} \tag{4}$$

Where x_g is the current longitudinal position of the contact patch on the road profile and is calculated from the values of $\mathbf{p_c}$, $\mathbf{x_p}$, and $\mathbf{n}$ at the previous time step. z_p is the height of the profile at the current time step and $R(x)$ is a user-defined function that returns the ellipsoid-filtered road profile height at position x. l_s is the contact patch half-length projected on the absolute x-axis and $\mathbf{e}$ is a constant unit vector pointing in the y-direction of the undisturbed wheel. $\mathbf{p_c}$ is the position on the ring of the contact point between the ring and the patch. $\mathbf{x_p}$ is the position of the patch, and $\mathbf{i}$, $\mathbf{j}$, and $\mathbf{k}$ are the standard unit vectors. Although $\mathbf{n}$ is the only variable of Eq. (2) that cannot be implicitly iterated it is deemed more appropriate to use previous time step data for $\mathbf{p_c}$ and $\mathbf{x_p}$ as well since it emulates a delay in the road profile instead of an iteration with a wrong value of $\mathbf{n}$.

3.5 Integration Scheme

In order to improve the simulation turnover time, an implicit integration scheme is used for the resolution of the tire forces. Thus, the forces from the magic formulae were implicitly integrated at each time step and the rotation parameters are handled by the updated-updated approach defined by Masarati [3]. A short explanation of the integration scheme of *MBDyn* is given in Sec. (5). The only exception to the implicit integration scheme is the road profile input. The road profile is integrated explicitly due to the fact that the normal direction and height of the road profile are functions of each other and would require a nested iterative loop within the code itself, as can be seen by Eqs. (2) and (3).

4 TRUCK MODEL

A precise distribution of the masses and modeling of the different dynamic components of the truck will allow retrieval of forces acting on the different truck components and evaluation of their fatigue. A simple driver algorithm is implemented in order to control the direction and velocity of the vehicle regardless of the road profile and of the drag.

The steer driver model used for the purpose of this analysis is a simple path follower model designed with a straight trajectory in mind. The purpose of the driver model is to maintain the proper orientation and position of the truck which is undergoing excitation by the road on which it is operating. It is achieved by controlling the angular velocity between the non-rotating node attached to the wheel node and the axle node.

The velocity of the truck model is controlled by the input torque at the wheels because the transmission line and motor losses will be taken into account outside of the dynamic model.

ISBN 978-2-8052-0116-5

A driving torque is applied when the velocity of the truck body is below the desired one; the magnitude of the torque is proportional to the offset of the truck body velocity. The purpose of the torque driver algorithm is to loosely represent the cruise control system of an average truck.

5 MBDYN

MBDyn is a free general-purpose multibody solver developed at the department of aerospace engineering of 'Politecnico di Milano' (`http://www.mbdyn.org/`).

It directly integrates in time Initial Value Problems (IVP) consisting of generic constrained mechanics problems. The structural analysis consists in writing Newton-Euler equations of motion of a set of rigid bodies,

$$\boldsymbol{M}(\boldsymbol{x})\dot{\boldsymbol{x}} = \boldsymbol{q} \qquad \dot{\boldsymbol{q}} = \boldsymbol{f}(\boldsymbol{x}, \dot{\boldsymbol{x}}, t), \tag{5}$$

connected by deformable elements and kinematic constraints. The kinematic variables $\boldsymbol{x}$ include rotation parameters. The equations of motion consist in force and moment equilibrium of each body as functions of the momentum and momenta moment variables $\boldsymbol{h}$.

Deformable elements, e.g. geometrically exact, nonlinear Finite Element-like beams [2], 4-node shells [5], and Component Mode Synthesis elements, can be used to model arbitrarily complex structural components.

Kinematic constraints are explicitly added to the problem as algebraic relationships between the Cartesian coordinates $\boldsymbol{x}$ of the bodies, $\boldsymbol{\phi}(\boldsymbol{x}, t) = \boldsymbol{0}$. The constraints are enforced using Lagrange's multipliers $\boldsymbol{\lambda}$. The resulting Differential-Algebraic Equations (DAE),

$$\boldsymbol{M}(\boldsymbol{x})\dot{\boldsymbol{x}} = \boldsymbol{q} \qquad \dot{\boldsymbol{q}} + \boldsymbol{\phi}^T_{/\boldsymbol{x}}\boldsymbol{\lambda} = \boldsymbol{f}(\boldsymbol{x}, \dot{\boldsymbol{x}}, t) \qquad \boldsymbol{\phi}(\boldsymbol{x}, t) = \boldsymbol{0}, \tag{6}$$

are integrated in time using implicit A/L-stable multistep integration schemes [4].

Arbitrary rotations are dealt with using an incremental approach. The orientation of each body at a given time step is described using its orientation $\boldsymbol{R}_k$. The incremental orientation between two time steps is $\boldsymbol{R}_{k-1,k}$, such that $\boldsymbol{R}_k = \boldsymbol{R}_{k-1}\boldsymbol{R}_{k-1,k}$. Since the problem is solved using a predictor-corrector scheme, the incremental orientation $\boldsymbol{R}_{k-1,k}$ is decomposed as $\boldsymbol{R}_{k-1,k} = \boldsymbol{R}^{(0)}\boldsymbol{R}_\Delta$, where $\boldsymbol{R}^{(0)}$ is the predicted increment of orientation, which remains constant during the subsequent correction phase of the numerical solution, whereas $\boldsymbol{R}_\Delta$ is unknown. The operator $\boldsymbol{R}_\Delta$ is described in terms of the Cayley-Gibbs-Rodrigues parameters,

$$\boldsymbol{R}_\Delta = \boldsymbol{I} + \frac{4}{4 + \boldsymbol{g}\cdot\boldsymbol{g}}(\boldsymbol{g}\times\ + \frac{1}{2}\boldsymbol{g}\times\boldsymbol{g}\times), \tag{7}$$

a very efficient parametrization that does not use trigonometric operations [1]. As a consequence, the orientation increment is small with respect not only to the rotation that results in a singularity of the parametrization, π, but also to the order of the integration scheme, $\|\boldsymbol{g}\| = o(\Delta t^n)$, thus allowing significant simplifications in the formulation of the Jacobian matrix of the problem.

For example, when computing first-order perturbations like $\delta(\boldsymbol{R}\boldsymbol{v})$, matrix $\boldsymbol{R}_\Delta \cong \boldsymbol{I}$, since

$$\delta(\boldsymbol{R}\boldsymbol{v}) = \delta(\boldsymbol{R}_\Delta\boldsymbol{R}^{(0)}\boldsymbol{v}) = \boldsymbol{R}\delta\boldsymbol{v} - (\boldsymbol{R}\boldsymbol{v})\times\boldsymbol{\Gamma}\delta\boldsymbol{g} \cong \boldsymbol{R}^{(0)}\delta\boldsymbol{v} - (\boldsymbol{R}^{(0)}\boldsymbol{v})\times\delta\boldsymbol{g}, \tag{8}$$

where matrix $\boldsymbol{\Gamma}$, which allows to compute the rotation derivative with respect to the rotation parameters, i.e.

$$\delta\boldsymbol{R}\boldsymbol{R}^T = \delta\boldsymbol{R}_\Delta\boldsymbol{R}^T_\Delta = (\boldsymbol{\Gamma}(\boldsymbol{g})\delta\boldsymbol{g})\times, \tag{9}$$

ISBN 978-2-8052-0116-5

is defined as

$$\mathbf{\Gamma}(\boldsymbol{g}) = \frac{4}{4 + \boldsymbol{g} \cdot \boldsymbol{g}}(\boldsymbol{I} + \frac{1}{2}\boldsymbol{g} \times), \tag{10}$$

and can be approximated by the identity as well. Finally, $\delta\mathbf{\Gamma} \cong \mathbf{0}$.

6 VALIDATION

6.1 Tire Model

The validation of the tire model is done using one wheel fixed to an axle of which the orientation and position are fixed in all DoF except the forward movement. This setup is intended to simulate the popular laboratory experiments used in the industry where a wheel rotating on a large drum or on a rigid conveyor belt is fixed at a specific axle height and measurements its forward velocity, which is actually the backward velocity of the drum or conveyor, wheel angular velocity, axle load, and axle positions are measured. This type of model will later serve to tune the tire model to the data of the Michelin tires.

The first set of tests is done on a perfectly smooth road profile only disturbed by the presence of a trapezoidal cleat of fifty millimeter width and ten millimeter height, identical to the one used by Schmeitz [9]. The responses of the tire rolling at different axle heights and velocities are compared with those of Schmeitz. It should be noted that the masses of the ring and of the wheel are supported by the normal force to the ground and the fixed wheel axle, respectively. The axle is fixed by a position constraint and thus, in the vertical direction,

$$F_{az} + M_w g = F_n - M_r g \tag{11}$$

where F_{az} is the vertical force required to hold the wheel axle in position, F_n is the normal force at the patch and in its reference frame, M_w and M_r are the masses of the wheel and ring, respectively, and g is the standard gravity. Thus, the force between axle and wheel is given by F_{az} while both this force and the weight of the wheel maintain the height of the wheel constant.

Thus, for a height determined by $F_{az} \approx 4000N$ and a velocity of thirty-nine kilometers per hour we have the responses shown in Figs. (10) to (12) where time is zero at the onset of the cleat in the unfiltered profile. These three figures shown the normal axle force, the longitudinal wheel-ring force, and the wheel angular velocity. The normal axle force and the angular velocity qualitatively agree fairly well with the results of Schmeitz [9] considering that his results are for a car tire and the ones shown here are for a truck tire. One can notice that the response is stronger in the case of the truck tire and that the damping is lower. It should also be noted that the actual tire used is yet to be tuned with the data from the manufacturer. The discrepancy of the longitudinal force is explained by the fact that, in his experiments, Schmeitz, used a fixed axle velocity. However, in the current simulation the velocity is controlled by the input torque at the wheel and this implies that the wheel converts some of the energy fed by the longitudinal force into a velocity change.

In the Figs. (13) to (15), the forward kinetic energy captured by the wheel, where the simulated setup is different from the laboratory experiments, is plotted for the cases with and without torque controlled by the driver model. It is visible that the torque controlled wheel is slightly damped by the effect of the torque that acts to counter forward velocity losses and ends up

ISBN 978-2-8052-0116-5

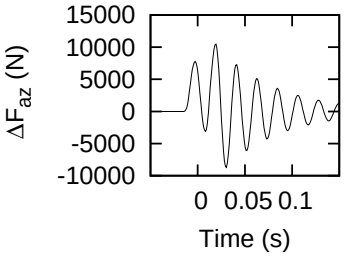

Figure 10: Normal force.

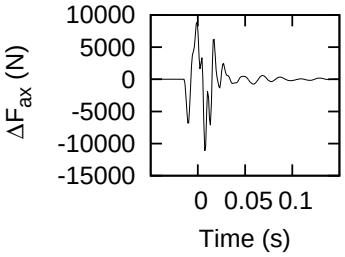

Figure 11: Longitudinal force.

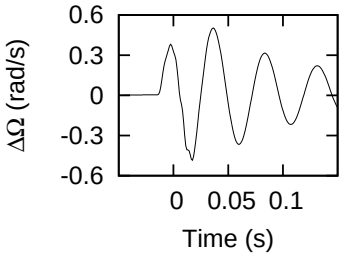

Figure 12: Angular velocity.

feeding energy to the wheel. To assess the energy difference of the road with cleat and without cleat requires a consideration of the angular velocities of the wheel and the ring, the forward velocity of the wheel, the velocities of the patch, and the deformation of the elastic elements. Also, great care as to be taken during the calibration of the model in order to properly represent the energy dissipation because the slip ratio is dependent on values which are influenced by the deformation of the viscoelastic elements within the model. This implies that an improper tuning can lead to misestimation of the friction forces. A plot of the longitudinal forces of the case with a torque control is also shown for reference purposes and it is seen that, for this case, the torque does not have a great influence on the longitudinal force response. The discrepancy can be explained by differences in tire properties.

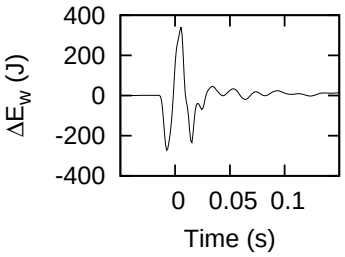

Figure 13: Forward kinetic energy.

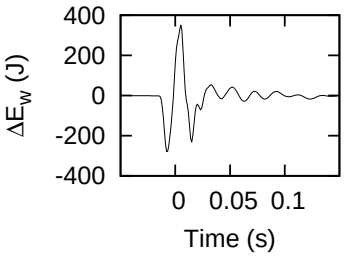

Figure 14: Energy without torque.

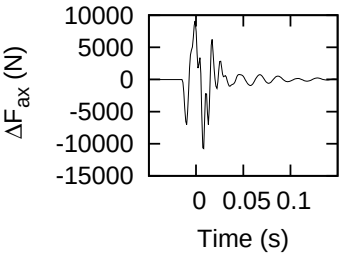

Figure 15: Force without torque.

6.2 Simplified Truck Model

An initial validation procedure is undertaken with a model consisting of a tractor body with one steering axle and one driving axle and a realistic suspension on each axle. The response to a lane change procedure undertaken at fifty-nine kilometers per hour with the torque drive being shutoff just before any steering is done is shown in Figs. (16) to (19). As mentioned by Pacejka [7], the response of a SWIFT-type model should be identical to the magic formulae response at steady state and match fairly well for frequencies of disturbance up to 10 Hz. Thus, as expected, the response of this procedure mimic the one seen for the bicycle model of Sec. (2.2) that relied on the magic formulae only. Some differences are noticed. Amongst these is the initially opposite direction of the body yaw acceleration which is explained by the addition of the aligning torque formula to the tractor model. The aligning torque initially works against the lateral force before oscillating and fading out. Another difference is the oscillatory behavior of the response and that is expected from a rigid ring model. An example of such a response to step steer angle variations of a single wheel is shown by Maurice [6] and one can notice the

ISBN 978-2-8052-0116-5

similitude of his responses for a lane change induced by step steer inputs to the ones shown here. The lateral forces are also shown for the left front and rear wheels. The front, steering, wheel response compares well with the experiments of Maurice. The forces shown here are those between the wheel and the axle expressed in the reference frame of the wheel, which means that it follows steer for the front wheel. When compared to the bicycle model, a delay is noticed for the force of the rear truck wheel to vanish; it is attributed to the transient property of the rigid ring tire model. Other differences between the two models come from differences in the mechanical properties between the truck model and the bicycle model.

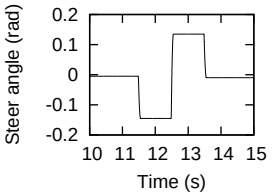

Figure 16: Steer angle.

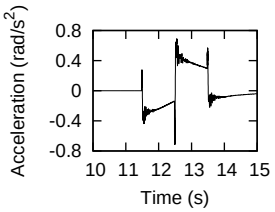

Figure 17: Body yaw.

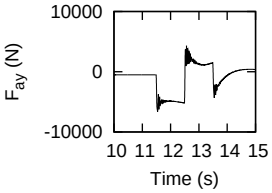

Figure 18: Front wheel.

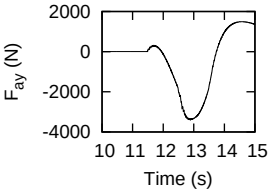

Figure 19: Rear wheel.

6.3 Tractor-Trailer Rig Model

A cab over engine tractor and a standard trailer are modeled with *MBDyn* and a model validation procedure is done. The tractor and trailer combination is modeled using a fairly standard approach since the main objective here is to have an improved tire model and test it. As can be seen on the side view of the three-dimensional truck model shown in Fig. (20), a detailed mass distribution of the tractor is taken into account. It is broken down between the viscoelastically connected axles, the tractor frame and the rigidly attached components, the engine, the driver, and the radiator. The tractor and trailer are connected by a spherical hinge joint, which could be changed to a joint that prevents relative rotation in roll between the tractor and trailer, in order to mimic the high torsional stiffness of the fifth wheel in that direction. The radiator body is free to move and rotate in all directions except the relative rotation about the y-axis; this restriction is achieved by a cardano rotation joint. The axles are allowed to rotate about the x-axis and move along the vertical axis, with respect to the frames of the tractor and trailer; this restriction is achieved by the combination of an in-line joint and a revolute rotation joint between each axle and the frame it is connected to. The engine and cabin are totally unconstrained and are supported by four three-dimensional viscoelastic elements, each. The driver is suspended on a chair which has a one-dimensional viscoelastic element in the vertical direction and is maintained in the same orientation and horizontal position as the cabin by means of a prismatic joint combined with an in-line joint. Each wheel is modeled using the rigid ring model developed for this project.

As for the simple truck model, the motion resulting from a lane change procedure is plotted in Figs. (21) to (24) and although the calibration of the model has not yet been done, one can notice that the expected behavior of the truck during the lane change is reproduced. The procedure is done at a velocity of sixty-two kilometers per hour and the steering angle function of time is exactly the same as for the simple truck model discussed before. The oscillations in the acceleration of the center of gravity of the tractor and of its middle axle, also shown, are assumed to come from the response of the suspension to the abrupt procedure. Finally,

ISBN 978-2-8052-0116-5

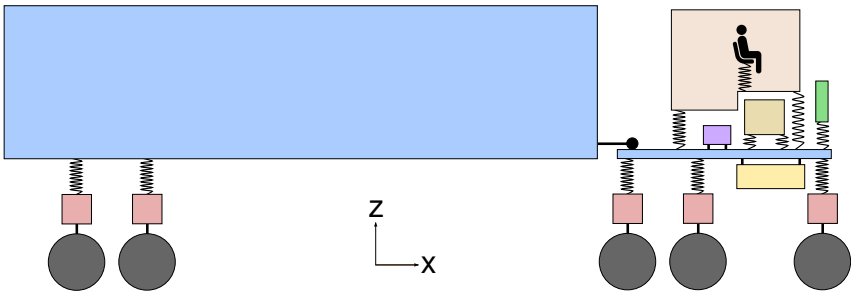

Figure 20: Side view of the three dimensional tractor-trailer rig.

the figures show that the trailer acts here in a similar fashion that the rear wheel did for the simple model. The axle and tractor yaw accelerations are fairly similar and show some strong oscillations, perhaps an indication of a lane change maneuver that is too aggressive.

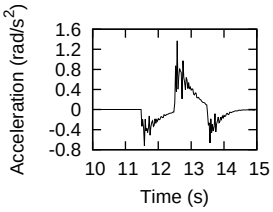

Figure 21: Body yaw.

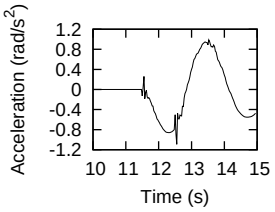

Figure 22: Trailer yaw.

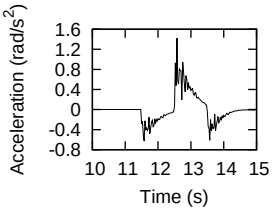

Figure 23: Axle yaw.

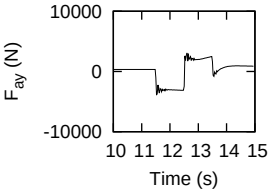

Figure 24: Front wheel.

7 CONCLUSION

A rigid ring tire model has been developed and the logic behind it was presented in this paper. The model was found to work as expected. Although the model was adequate for integration within a multibody software because it comprises many standard elements of multibody dynamics, many extra operations had to be made in order to implement, amongst others, the magic formula forces, the rotating parts that have non-rotating viscous elements, the interaction with the road, and the implicit integration scheme. Again, the truck model will be used for the evaluation of different road profiles in terms of energy consumption, vehicle wear, and driver safety, comfort, and health. Future work includes tuning the tire model to the experimental data, tuning the tractor-trailer rig model to field tests, and possibly adding a parameter for the dependence of the tire effective radius on velocity. Possible improvements to the tire model could include the adaptation to camber, consideration of combined slip effects, modeling of the loss of contact with the road, and model stability at low velocities. However, these improvements were not deemed necessary for the range of operation of the test cases to come.

8 ACKNOWLEDGEMENTS

The authors acknowledge the financial support of the Natural Sciences and Engineering Research Council of Canada and all the partners of its Industrial Research Chair on heavy loads / weather / pavement interaction (i3C). The support of Michelin, Freightliner, and Manac is also acknowledged for kindly accepting to provide technical data on their products.

ISBN 978-2-8052-0116-5

REFERENCES

[1] O. A. Bachaud and L. Trainelli. The vectorial parameterization of rotation. *Nonlinear Dynamics*, 32(1):71–92, 2003.

[2] G. L. Ghiringhelli, P. Masarati, and P. Mantegazza. A multi-body implementation of finite volume beams. *AIAA Journal*, 38(1):131–138, 2000.

[3] P. Masarati. *Comprehensive Multibody AeroServoElastic Analysis of Integrated Rotorcraft Active Controls*. PhD thesis, Politecnico di Milano, 2000.

[4] P. Masarati, M. Lanz, and P. Mantegazza. Multistep integration of ordinary, stiff and differential-algebraic problems for multibody dynamics applications. In *XVI Congresso Nazionale AIDAA*, pages 1–10, Palermo, 24–28 September 2001.

[5] P. Masarati, M. Morandini, G. Quaranta, and R. Vescovini. Multibody analysis of a micro-aerial vehicle flapping wing. In *Multibody Dynamics 2011*, Brussels, Belgium, 4-7 July 2011.

[6] J. P. Maurice. *Short Wavelength and Dynamic Tyre Behaviour under Lateral and Combined Slip Conditions*. PhD thesis, Delft University of Technology, 2000.

[7] H. B. Pacejka. *Tire and vehicle dynamics*. Society of Automotive Engineers, 2006.

[8] M. Sayers. Development, implementation, and application of the reference quarter-car simulation. In *Measuring road roughness and its effects on user cost and comfort*, pages 25–47. American Society for Testing and Materials, 1985.

[9] A. J. C. Schmeitz. *A Semi-Empirical Three-Dimensional Model of the Pneumatic Tyre Rolling over Arbitrarily Uneven Road Surfaces*. PhD thesis, Delft University of Technology, 2004.

[10] P. W. A. Zegelaar. *The Dynamic Response of Tyres to Brake Torque Variations and Road Unevennesses*. PhD thesis, Delft University of Technology, 1998.

ISBN 978-2-8052-0116-5